Talanta 88 (2012) 136–144

Contents lists available at SciVerse ScienceDirect

Talanta

journal homepage: www.elsevier.com/locate/talanta

NMR analysis of the rat neurochemical changes induced by middle cerebral artery occlusion

Mingxing Yang[a,b], Shu Wang[c], Fuhua Hao[b], Yajie Li[d], Huiru Tang[b,*], Xuemin Shi[a,**]

[a] First Affiliated Hospital of Tianjin University of Traditional Chinese Medicine, Tianjin University of Traditional Chinese Medicine, Tianjin, 300193, China
[b] State Key Laboratory of Magnetic Resonance and Atomic and Molecular Physics, Wuhan Centre for Magnetic Resonance, Wuhan Institute of Physics and Mathematics, Chinese Academy of Sciences, Wuhan, 430071, China
[c] Tianjin Key Laboratory of Acupuncture and Moxibustion, First Affiliated Hospital of Tianjin University of Traditional Chinese Medicine, Tianjin University of Traditional Chinese Medicine, Tianjin, 300193, China
[d] Department of Chinese Medicine, Beijing Chao-Yang Hospital, Capital Medical University, Beijing, 100020, China

ARTICLE INFO

Article history:
Received 11 July 2011
Received in revised form 9 October 2011
Accepted 16 October 2011
Available online 25 October 2011

Keywords:
Metabonomics
Focal cerebral ischemia
MCAO
Pattern recognition
NMR spectroscopy
Neurochemistry

ABSTRACT

Stroke is a leading cause of death and disability, affecting millions of people worldwide with almost 80% of them as ischemic stroke and understanding the multiple mechanisms underlying cerebral ischemia is essential for development of effective treatments. To understand metabolic changes induced by focal brain ischemia, we conducted a comparative analysis of metabolic composition of cerebral tissue from rats with sham-operation and middle cerebral artery occlusion (MCAO) using high-resolution nuclear magnetic resonance (NMR) spectroscopy. More than 40 metabolites were assigned including organic acids, amino acids, carbohydrates, choline, pyrimidine and purine metabolites. Our results showed that MCAO led to significant level decreases for glutamate, glutamine, aspartate, γ-aminobutyrate (GABA), taurine, malate, fumarate, acetate, phosphocreatine, and purine and pyrimidine metabolites such as inosine, hypoxanthine, xanthine, uracil and UDP/UTP, together with significant level increases for glucose in focal brain tissue extracts. This demonstrated that experimental ischemic stroke in rats caused extensive perturbation in tricarboxylic acid cycle, GABA shunt, and metabolisms of choline and nucleic acids. These findings provided essential information for our understandings of MCAO-caused biochemical alterations and demonstrated the metabolite composition analysis as a useful tool for understanding the neurochemistry of stroke.

1. Introduction

Stroke is a serious cause of both morbidity and mortality affecting the health of over 16 million people worldwide every year [1] and has become a heavy burden on both the concerned families and community. To be more specific, more than 5 million man and women died and another 5 million were disabled by stroke annually [2]. In United States alone, the direct and indirect costs caused by stroke were estimated to be more than 40 billion U.S. dollars in 2007 [3]. The total losses caused by ischemic stroke from 2005 to 2050 is projected to reach 2.2 trillion dollars [4]. With the rise of aging population, the burden will also be increased greatly in developing countries including China. Almost 80% of all strokes are ischemic cerebral events in both developed and developing countries [5]. Despite the prevalence and severe consequences, however, there are few effective treatments available for ischemic stroke. The only FDA-approved clot-busting drug, tissue plasminogen activator, is required to be administered within 3 h from the onset of stroke. However, such requirement is not easy to meet. In United State, for instance, only less than 5% ischemic stroke patients can reach hospitals in time and be considered for this treatment. So far, the pathogenesis is not clearly understood and thus comprehension of the stroke related pathophysiology is essential for disease prediction and effective therapeutic screening to minimize the severity of ischemic damage.

Focal brain ischemia results from an abrupt blood flow reduction below a critical threshold because of obstruction of a major brain artery. The restricted delivery of oxygen and glucose impairs the ATP synthesis and this energy failure can cause the ischemic cascades such as acidosis [6], inflammation [7], production of reactive oxygen species [8], necrosis, apoptosis and eventually neuronal death [9]. Metabolic disturbance plays an important role in brain ischemic injury, including an increase in anaerobic glycolysis, excessively release of glutamate to extracellular space [10], perturbation of glutamate–glutamine cycle [11] and turnover of

* Corresponding author. Tel.: +86 027 87198430; fax: +86 027 87199291.
** Corresponding author. Tel.: +86 022 27432011; fax: +86 022 27432227.
E-mail addresses: 2002ymx02@163.com (M. Yang), wshu2002@hotmail.com (S. Wang), haofuhua78@163.com (F. Hao), LYJ_Jolly@hotmail.com (Y. Li), huiru.tang@wipm.ac.cn (H. Tang), tjdrshi@msn.com (X. Shi).

0039-9140/$ – see front matter © 2011 Elsevier B.V. All rights reserved.
doi:10.1016/j.talanta.2011.10.022

protein synthesis [12]. Therefore, metabolic analysis ought to be a useful approach for understanding the biochemical aspects of stroke.

Magnetic resonance spectroscopy (MRS) has been proven as a powerful tool to investigate the metabolic alterations in ischemic stroke *in vivo*. Previous *in vivo* studies showed that cerebral ischemia led to the level changes in lactate, creatine, N-acetylaspartate (NAA) and choline [13–16]. However, with low sensitivity and limited resolution, the detectable and assignable metabolites from MRS were limited. High-resolution nuclear magnetic resonance (NMR) spectroscopy offers a better alternative to acquire more metabolic information since these techniques are capable of simultaneously detecting a wide range of metabolites and their changes associated with physiological and genetic alterations. Multivariate data analysis approaches [17–19], such as principal component analysis (PCA) and orthogonal partial least squares discriminant analysis (OPLS-DA), are normally employed to uncover and visualize the metabolic alterations relative to the biological disturbance of interests. Such combination has become the technical basis for so-called metabonomics [20,21]. In practice, metabonomics typically makes use of high-resolution NMR or mass spectrometry (MS) analyses to provide metabolic profiles of biological samples such as urine, blood and seminal fluid. Consequently, metabonomics has been successfully used as an important tool for understanding pathophysiology [22–25], identifying biomarkers [26,27], disease diagnosis [23,28] and mechanistic aspects of toxicity [29–31].

MCAO has been employed as one of classic models to study the pathogenesis of focal brain ischemia in term of changes in gene expression, transcriptions and proteins. More recently, NMR and high performance liquid chromatography (HPLC) were used to observed metabolic changes under ischemic condition. These works showed that cerebral ischemia caused level increases for adenosine at 4 h [32] and for inosine and hypoxanthine 6 h after occlusion in extracellular fluid of striatum [33].

Elevation of acetate and decreases of glutamine and aspartate were also observed in the ischemic tissue 6 h after occlusion [34–36]. NMR measurements of cerebral ischemic tissue extracts indicated that focal ischemia caused decrease in aspartate, glutamate, NAA and total creatine at 24 h after occlusion [34]. However, these studies were fragmented in terms of the metabolisms and the holistic metabolic responses of cerebral tissues to focal brain ischemia remained to be fully understood.

In this work, we applied the NMR-based metabonomic strategy to search for the metabolic variations in ischemic brain tissue following experimental stroke induced by an intraluminal filament occlusion of the middle cerebral artery. The aim of this study is to further define the metabolic features associated with the occlusion of middle cerebral artery.

2. Materials and methods

2.1. Chemicals

2,3,5-Triphenyltetrazolium chloride (TTC) was purchased from Sigma–Aldrich Co. (St. Louis, MO, USA). Sodium chloride, $K_2HPO_4{\cdot}3H_2O$ and $NaH_2PO_4{\cdot}2H_2O$ (all in analytical grade) were obtained from Sinopharm Chemical Reagent Co., Ltd. (Shanghai, China); D_2O (99.9% in D) and sodium 3-trimethlysilyl [2,2,3,3-D_4] propionate (TSP) were purchased from Cambridge Isotope Laboratories (Miami, FL). K_2HPO_4/NaH_2PO_4 buffer (0.1 M, pH 7.4) was employed for NMR studies due to their good solubility and storage stability [37], which contained D_2O (10%, v/v) as a field lock and TSP (0.03 mM) as chemical shift reference.

2.2. Animal handling

Animal procedures were conducted in accordance with the National Guidelines for Experimental Animal Welfare (Ministry of Science and Technology of People's Republic of China, 2006). Male Sprague-Dawley rats were purchased from Vital River Laboratories (Beijing, China) and housed in groups of five and allowed to acclimate for at least five days in a temperature-controlled environment (24 °C) with lighting between 07:00 and 19:00. All animals had free access to food and water throughout the study and were randomly assigned to sham-operated and MCAO groups with body weigh of 248–260 g after acclimation.

2.3. Focal brain ischemia models

Permanent focal cerebral ischemia was induced using the filament model as described previously [38]. Briefly, rats were anesthetized with 10% chloral hydrate. Through a midline neck incision, the right external and internal carotid arteries were dissected from the surrounding connective tissue. A nylon monofilament coated with paraffin wax was inserted into the right common carotid artery and advanced into the right internal carotid artery until mild resistance was felt, indicating that the filament was positioned properly and occluded blood flow to the middle cerebral artery. Sham-operated rats were subjected to the same surgical procedure except that filaments inserted into the right common carotid artery were 0.5 cm. Nylon monofilaments were soaked in gentamicin injection and saline for 30 min, respectively, and washed with saline before used. All surgical procedures were kept in a sterile environment. The operated animal body temperature was kept about 37 °C until neurological evaluation. Neurological evaluation was performed 2 h and 26 h after occlusion of middle cerebral artery according to a 5-points scale described in a previous report [39]. Briefly, a score of 0 means no neurological deficit; a score of 1 indicates failure to extend left forepaw fully; a score of 2 means circling to the left on the ground; a score of 3 means falling to the left when walking; rats with a score of 4 could not walk spontaneously and with disturbance of consciousness. Rats scored 1–3 at 2 h post occlusion were considered as successful MCAO models.

In order to estimate the infarct volume for tissue extraction, three rats were subjected to MCAO with infarct volume visualized by TTC staining as previously described [39]. Briefly, 2 mm-thick coronal sections of brain tissue were stained in 2% TTC for 30 min at 37 °C following 12 h immersion in 10% formalin. Normal cerebral tissue was stained red whereas the infarct tissue unstained.

2.4. Tissue extraction procedure

Twenty-six hours after insertion of filaments, rats were sacrificed with decapitation and brain tissues were quickly removed, snap-frozen in liquid nitrogen and stored at −80 °C until further analysis. During extraction, the ischemic part of right brain supplied blood flow by the middle cerebral artery was removed, weighed and then ground in liquid nitrogen. 600 μl CH_3OH/H_2O (1:1) was added to the ground brain tissue and allowed to thaw for 10 min followed with 30 s intermittent sonication (10 s sonication and 10 s break, repeated for three times) in an ice bath. After centrifugation at 11180 × *g* at 4 °C for 10 min, the supernatant was transferred into a new EP tube and the pellet was re-extracted twice with the same procedure. The supernatants from three extractions were combined. Methanol was removed from the pooled supernatant under vacuum in a Savant SpeedVac concentrator (Thermo SAVANT, SC110A-230) for 18 h and then lyophilized in a freeze-drier for at least 24 h. The dried powder samples were added with 600 μl Na–K phosphate buffer (0.1 M, pH 7.4) containing 10% D_2O and 0.03 mM TSP. After centrifugation (11180 × *g*) at 4 °C for 5 min,

550 μl of supernatant was transferred into a 5 mm NMR tube for NMR measurements.

2.5. NMR analysis

All ^{1}H NMR spectra were acquired at 298 K on a Bruker AVIII-600 NMR spectrometer equipped with a 5 mm inverse cryogenic probe (Bruker Biospin, Germany), operating at 600.13 MHz for ^{1}H. One-dimensional NMR spectra were recorded using the first increment of NOESY pulse sequence (RD–90°–t_1–90°–t_m–90°–acquisition). Water suppression was achieved with a weak continuous wave irradiation on the water peak during the recycle delay (RD, 2 s) and mixing time (t_m, 100 ms). t_1 was set to 4 μs. The 90° pulse length was adjusted to about 10 μs for each sample. The spectral width was set to 20 ppm, and a total of 64 scans were collected into 32k data points for each spectrum. The free induction decays (FIDs) for one-dimensional data were zero-filled to 128k data points and multiplied by an exponential function with a line-broadening factor of 1 Hz prior to Fourier transformation (FT).

For signal assignment purposes, two-dimensional (2D) NMR spectra were also acquired at 298k on a Bruker AVIII-800 MHz spectrometer for selected samples including ^{1}H–^{1}H correlation spectroscopy (COSY), total correlation spectroscopy (TOCSY), J-resolved spectroscopy (JRES), ^{1}H–^{13}C heteronuclear single quantum coherence spectroscopy (HSQC) and heteronuclear multiple-bond correlation (HMBC). This NMR spectrometer was also equipped with a 5 mm inverse cryogenic probe but operated at 800.20 MHz for ^{1}H and 201.23 MHz for ^{13}C. In COSY and TOCSY experiments, 64 transients were collected into 2048 data points for each of 160 increments with the spectral width of 10.5 ppm for both dimensions. Phase insensitive mode with gradient selection was used for the COSY experiments and the well-known MLEV-17 was employed as the spin-lock scheme in the phase sensitive TOCSY experiment (TPPI) with the mixing time of 85 ms. For JRES spectra, 64 transients were collected into 4096 data points for each of 80 increments with spectral width of 8417 Hz in the acquisition and 60 Hz in the evolution dimensions. ^{1}H–^{13}C HSQC and HMBC 2D NMR spectra were recorded using the gradient selected sequences with 480 transients and 2048 data points for each of 128 increments. The spectral widths were set 8418 Hz for ^{1}H, 35,215 Hz for ^{13}C in HSQC and 44,271 Hz for ^{13}C HMBC experiments, respectively. The data were zero-filled to a 2 × 2k matrix with appropriate window functions prior to FT.

2.6. NMR data processing and multivariate data analysis

^{1}H NMR spectra of brain extracts were manually corrected for phase and baseline distortions, and referenced to TSP (δ0.0) using software package TOPSPIN (V2.0, Bruker Biospin, Germany). The spectral region δ0.5–9 was bucketed into 16,999 bins (0.3 Hz each) using software AMIX (V3.8.3, Bruker Biospin, Germany). The regions of δ4.5–5.2 and δ3.34–3.39 were discarded to eliminate the effects of imperfect water suppression and residual methanol signal. Each integrated NMR spectral bin was normalized to the corresponding weight of brain tissue. The normalized NMR spectral data were imported into SIMCA-P+ (V12, Umetrics, Sweden) for multivariate data analysis. Principal component analysis was first carried out on the initial data with pareto scaling to generate an overview and to find possible outliers. Results were then visualized in the form of the scores plots in which each point represented an individual sample. OPLS-DA was performed with 7-fold cross-validation [40] on the same data with pareto scaling using the NMR data as X-matrix and the class information as Y-variables. The quality of OPLS-DA models were evaluated according to previous reports with R^2Y, the goodness of fit, Q^2Y, the goodness of prediction, and the difference between R^2Y and Q^2Y [41]. The significance of OPLS-DA model was further tested using CV-ANOVA [42]. Coefficient-coded loadings plots were generated using an in-house developed MATLAB (Version 7.0.1.14, The MathWorks, MA) script to search for significantly changed metabolites related to focal cerebral ischemia. In OPLS-DA coefficient plots, the back-transformed loadings of the predictive component was used to preserve the original NMR spectral appearance, where the direction of peaks indicated the direction of increase (upward) or decrease (downward) in metabolite concentration with respect to the predefine classes [43]. The statistical significance of metabolites was also confirmed by two-side unpaired t-test of the sum of intensity from specific protons of metabolite ($p < 0.05$). In addition, the relative changes of metabolites in the MCAO model were calculated using the normalized NMR data in comparison with the sham group, i.e., $(C_M - C_s)/C_s$, where C_M stands for the mean metabolite concentration of MCAO group and C_s the sham group.

3. Results

3.1. Evaluation of animal models

The neurological deficit scores (Table S1) indicated that MCAO was successfully induced in nine animals with three rats scored similarly to the sham group. Seven sham-operated rats all had no neurological deficit with a score of 0 at 2 h and 26 h after operation. All rats were alive at 26 h after occlusion.

3.2. Metabolite assignments of ^{1}H NMR spectra

Fig. 1 shows the typical ^{1}H NMR spectra of brain tissue extracts obtained from sham (A) and MCAO (B) rats 26 h after operation. Assignments of ^{1}H and ^{13}C resonances to specific metabolites were made (Table 1) based on the literatures data [44,45], publically accessible database [46] and further confirmed by JRES, ^{1}H–^{1}H COSY, ^{1}H–^{1}H TOCSY, ^{1}H–^{13}C HSQC and ^{1}H–^{13}C HMBC 2D NMR spectra as previously reported [60,61]. The NMR spectra of brain tissue extracts contained more than 40 assignable metabolites, including three organic acids, five intermediates of Krebs cycle, sixteen amino acids and some short-chain fatty acids. Glycerol, creatine and glucose were also detected together with four pyrimidine and purine metabolites (i.e., hypoxanthine, xanthine, inosine and uracil) and four unknown metabolites (Fig. 1, Table 1).

3.3. Validity of OPLS-DA models

PCA scores plot (Fig. 2A) showed a moderate separation for the sham and successful MCAO animals (Fig. 2A) with the first two principal components explaining 93.7% of variances of NMR spectra, in which no outliers were found. Comparative OPLS-DA model was calculated for the sham and MCAO groups with one predictive and one orthogonal component. A clear separation was obtainable for these two groups (Fig. 2C) with a valid model indicators ($R^2X = 0.936$, $R^2Y = 0.914$, $Q^2Y = 0.877$). The difference between R^2Y and Q^2Y was only 0.037. The CV-ANOVA result further showed that the OPLS-DA model was highly significant ($p = 5.63 \times 10^{-5}$). A new PCA model calculated with data from all animals showed that those three animals failed to get neurological deficits in the MCAO group clustered with the sham group (Fig. 2B). When the above OPLS-DA model was used to predict the groupings, these three animals were also classified into the sham group (Fig. 2D).

3.4. Metabolic alterations induced by MCAO

The results from the back-transformed OPLS-DA coefficient plot and the p-values of two-side unpaired t-test showed that levels

Table 1
^{1}H and ^{13}C NMR data for metabolites from brain extracts of MCAO and sham rats.

Keys	Metabolites	Group	δ^{1}H (multiplicity)[a]	δ^{13}C	Experiments
1	Isoleucine	γ-CH_3	0.94(t)	13.9	JRES, TOCSY, HSQC
		δ-CH_3	1.01(d)	17.6	
		γ′-CH_2	1.48(m)	24.5	
		β-CH	1.95(m)	38.6	
		α-CH	3.67(d)	62.6	
2	Leucine	δ-CH_3	0.96(d)	24.0	JRES, TOCSY, HSQC
		δ′-CH_3	0.97(d)	24.8	
		γ-CH	1.70(m)	42.7	
		β-CH_2	1.72(m)	29.2	
		α-CH	3.74(t)	56.9	
3	Valine	γ′-CH_3	0.99(d)	19.6	JRES, TOCSY, HSQC
		γ-CH_3	1.05(d)	20.9	
		β-CH	2.28(m)	32.1	
		α-CH	3.62(d)	63.5	
4	U4	C-H_3	1.15(d)	21.7	JRES, HSQC
5	β-Hydroxybutyrate	γ-CH_3,	1.20(d)	24.5	JRES, TOCSY, HSQC, HMBC
		α-CH_2	2.34(m)	–	
		α′-CH_2	2.41(m)	–	
		C-H	4.12(m)	67.2	
6	Lactate	β-CH_3,	1.33(d)	23.0	JRES, TOCSY, HSQC, HMBC
		α-CH	4.11(q)	71.5	
		COOH	–	185.1	
7	Alanine	β-CH_3	1.48(d)	19.2	JRES, TOCSY, HSQC, HMBC
		α-CH	3.79(q)	53.6	
		COOH	–	178.9	
8	Lysine	γ-CH_2,	1.48(m)	24.3	JRES, TOCSY, HSQC
		δ-CH_2	1.73(m)	29.3	
		β-CH_2	1.91(m)	32.2	
		ε-CH_2,	3.03(t)	42.4	
		α-CH	3.76(t)	57.7	
9	GABA	β-CH_2	1.91(q)	26.8	JRES, TOCSY, HSQC, HMBC
		α-CH_2	2.30(t)	37.1	
		γ-CH_2	3.02(t)	42.4	
		COOH	–	184.4	
10	Acetate	CH_3	1.92(s)	26.3	JRES, HSQC, HMBC
		COOH	–	184.3	
11	Glutamate	β′-CH	2.06(m)	29.9	JRES, TOCSY, HSQC
		β-CH	2.13(m)	29.9	
		γ-CH_2	2.35(dt)	36.3	
		α-CH	3.76(t)	57.6	
12	Glutamine	β-CH_2	2.14(m)	29.6	JRES, TOCSY, HSQC, HMBC
		γ-CH_2	2.45(m)	33.8	
		α-CH	3.78(m)	57.3	
		COOH	–	177.3	
13	Malate	β′-CH	2.37(dd)	45.8	JRES, TOCSY, HSQC, HMBC
		β-CH	2.68(dd)	45.8	
		α-CH	4.31(dd)	73.4	
		COOH	–	179.6	
14	α-Ketoglutarate	β-CH_2	2.45(t)	33.7	JRES, TOCSY, HSQC
		γ-CH_2	3.01(t)	39.9	
15	Citrate	CH_2	2.55(d)	48.4	JRES, TOCSY, HSQC
		CH_2	2.67(d)	48.4	
16	Aspartate	β-CH	2.68(dd)	39.6	JRES, TOCSY, HSQC, HMBC
		β′-CH	2.82(dd)	39.6	
		α-CH	3.91(dd)	55.2	
		γ-COOH	–	176.9	
		COOH	–	180.3	
17	Creatine/phosphocreatine	CH_3	3.04(s)	39.8	JRES, TOCSY, HSQC, HMBC
		CH_2	3.94(s)	56.7	
		N═C	–	160.1	
		COOH	–	177.3	
18	Ethanolamine	NH-CH_2	3.15(t)	44.5	JRES, TOCSY, HSQC
		HO-CH_2	3.83(t)	60.7	
19	Choline	N-$(CH_3)_3$	3.21(s)	56.9	JRES, TOCSY, HSQC
		β-CH_2	3.52(t)	70.3	
		α-CH_2	4.07(t)	58.6	
20	Phosphorylethanolamine	N-CH_4	3.23(t)	42.6	JRES, TOCSY, HSQC
		O-CH_2	3.99(m)	63.3	
21	*Myo*-inositol	5-CH	3.29(t)	77.1	JRES, TOCSY, HSQC
		1,3-CH	3.55(dd)	74.3	
		4,6-CH	3.63(dd)	75.3	
		2-CH	4.07(t)	75.1	
22	Taurine	N-CH_2	2.27(t)	38.5	JRES, TOCSY, HSQC
		S-CH_2	3.42(t)	50.6	
23	β-Glucose	2CH	3.25(t)	77.1	JRES, TOCSY, HSQC
		4CH	3.41(dd)	72.6	

Table 1 (*Continued*)

Keys	Metabolites	Group	δ^1H (multiplicity)[a]	δ^{13}C	Experiments
		5CH	3.47(m)	78.8	
		3CH	3.49(t)	78.8	
		6CH	3.74(dd)	63.8	
		6CH	3.91(dd)	63.8	
		1CH	4.65(d)	98.8	
24	α-Glucose	1CH	5.24(d)	95.1	JRES, TOCSY, HSQC
		2CH	3.54(dd)	74.4	
		3CH	3.73(dd)	75.5	
		4CH	3.42(t)	72.6	
		5CH	3.84(m)	63.6	
25	U1	–	3.47(s)	54.4	JRES, HSQC
26	Glycerol	CH_2	3.57(dd)	65.5	JRES, TOCSY, HSQC
		CH_2,	3.66(dd),	65.6	
		CH	3.79(m)	75.1	
27	Phosphorylcholine	N-$(CH_3)_3$	3.23(s)	56.9	JRES, TOCSY, HSQC
		N-CH_2	3.60(m)	69.1	
28	Dihydroxyacetone	CH_2	4.43(s)	67.9	JRES, HSQC
29	U2	–	5.62(d)	–	JRES, TOCSY
		–	4.05(m)	–	
		–	4.09(d)	–	
30	Glycine	α-CH	3.57(s)	44.5	JRES, HSQC, HBMC
		COOH	–	175.2	
31	Uracil	5-CH	5.81(d)	103.9	JRES, TOCSY, HSQC
		6-CH	7.55(d)	146.5	
32	Inosine	1-CH	6.10(d)	–	JRES, TOCSY
		8-CH	8.24(s)	–	
		14-CH	8.35(s)	–	
33	Fumarate	CH	6.53(s)	138.1	JRES, HSQC
34	Tyrosine	CH	6.91(dd)	118.8	JRES, TOCSY, HSQC
		CH	7.20(dd)	133.7	
35	Phenylalanine	4-CH	7.33(dd)	132.1	JRES, TOCSY, HSQC
		3,5-CH	7.38(dd)	130.8	
		2,6-CH	7.43(m)	132.0	
36	Xanthine	H	7.90(s)	143.3	JRES, HSQC
37	Nicotinurate	5-CH	7.60(m)	–	JRES, TOCSY
		4-CH	8.25(dd)	–	
		6-CH	8.72(dd)	–	
		2-CH	8.95(t)	–	
38	Hypoxanthine	2-CH	8.20(s)	148.4	JRES, HSQC
		8-CH	8.22(s)	144.9	
39	Formate	CH	8.46(s)	–	JRES
40	Threonine	γ-CH_3	1.33(d)	23.0	JRES, TOCSY, HSQC, HMBC
		α-CH	3.59(d)	63.6	
		β-CH	4.26(m)	69.0	
		COOH	–	175.9	
41	UDP/UTP[b,c]	CH	5.99(d)	–	JRES, TOCSY
		CH	7.96(d)	–	
		CH	4.38	–	
42	Phosphoenolpyruvate	CH_2	5.19(d)	96.8	JRES, TOCSY, HSQC
		CH_2	5.38(d)	97.1	
43	Histidine	3-CH	7.09(d)	120.0	JRES, TOCSY, HSQC
		5-CH	7.86(d)	138.9	
44	U3	–	8.00(d)	–	JRES, TOCSY
45	Succinate	CH_3	2.41	37.2	JRES, HSQC
46	Serine	α-CH	3.85(dd)	59.3	JRES, HSQC, HMBC
		β-CH_2	3.99(m)	63.3	
		COOH	–	175.2	

[a] Multiplicity: s, singlet; d, doublet; dd, double of doublets; t, triplet; q, quartet; m, multiplet; U, unidentified signals; –, signals or multiplicities were not detected.
[b] Tentatively assigned.
[c] UDP/UTP, uridine diphosphate/uridine triphosphate.

of 21 metabolites changed significantly in the ischemic brain tissue compared with sham group (Fig. 3, Table 2). Glucose level was markedly elevated in the MCAO samples (for more than 5 folds). Level decreases were observable for aspartate, taurine, glutamate, glutamine, GABA, acetate, creatine, choline, *myo*-inositol, phosphorylcholine, nicotinurate, hypoxanthine, xanthine, inosine, uracil and UDP/UTP. Furthermore, the levels for the intermediates of TCA cycle, such as malate and fumarate, were also significantly reduced in the MCAO samples (Fig. 3, Table 2).

4. Discussions

The valid OPLS-DA model showed clear clustering for MCAO and sham groups indicating significant metabolic differences between two groups. These differences were highlighted by the MCAO-induced elevation of glucose and depletion of glutamate, GABA, glutamine, acetate, aspartate, taurine, fumarate, malate, choline, phosphorylcholine, *myo*-inositol, creatine, uracil, inosine, hypoxanthine and xanthine (Fig. 3, Table 2).

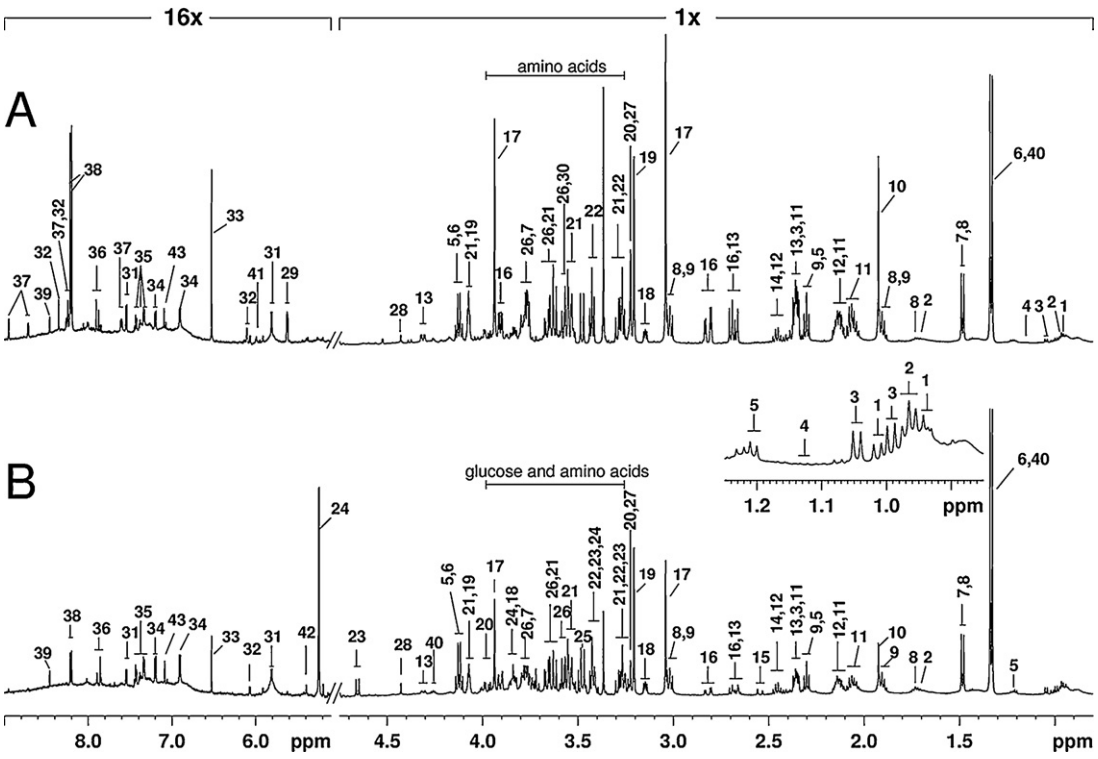

Fig. 1. Typical 600 MHz ^{1}H NMR spectra of brain tissue extracts obtained from a sham (A) and a MCAO (B) rats. The spectra region δ5.0–9.0 was vertically expanded for 16 times. The keys were given in Table 1.

It is known that as a major energy-consumer of carbohydrates and oxygen, brain is sensitive to anoxia/ischemia. Occlusion of middle cerebral artery causes the depleted supply of oxygen and glucose in focal brain tissue leading to the breakdown of aerobic glycolysis. During ischemia, the cellular ATP level drastically decreased in cerebral tissue accompanied by the depletion in the phosphocreatine concentration [47]. The reduced concentrations of fumarate and malate were observed in ischemic cerebral tissue (Table 2, Fig. 3) suggesting suppression of tricarboxylic acid cycle. The decrease in the level of phosphocreatine, a well-known reservoir of phosphate group for producing ATP, in the MCAO rats is consistent with previous report [48]. Malate-aspartate shuttle is one of principal systems that transfer NADH in the cytosol through the inner membrane to enter mitochondria for oxidative phosphorylation to generate ATP. The decreases in malate and aspartate observed here in the ischemic brain tissue indicated the decreased malate-aspartate shuttle activity. This is in good agreement with previous research report that the activity of the malate-aspartate shuttle has markedly decreased as soon as 10 min after brain ischemia [49]. The observation of the level elevation of glucose in MCAO group is probably due to the elevation of glucose at the edge of ischemic area and the depression of glucose utilization by brain cell, as suggested by previous report [50].

Glutamate and aspartate are excitatory amino acids that can stimulate postsynaptic neurons whereas GABA, taurine are inhibitory amino acids which can reduce excitability of neurotransmission. The homeostasis of metabolism in glutamate, GABA is often dependent on the interaction between neurons and astrocytes under the physiological conditions. Previous studies showed that the extracellular content of excitatory amino acids (glutamate and aspartate) and inhibitory amino acids (GABA, taurine) reached a maximum in rats 1–2 h after MCAO but began to decrease 3 h after MCAO [32,51]. In this work, the concentrations of glutamate, aspartate, GABA, taurine were decreased concurrently 26 h after MCAO being in good agreement with some of the previous observations [52]. Since taurine has a potential neuroprotective function [53], the decrease of taurine level in local cerebral tissue implied that MCAO also had negative effects on neuronal activities. These effects are probably associated with the depression of TCA cycle, malate–aspartate shuttle and glutamate–glutamine cycle, which is reflected with the MCAO-induced decreases of glutamine and glutamate.

The reduction of acetate concentration in ischemic brain indicated that glias suffered metabolic dysfunctions and probably neuron injuries during ischemia. This is because acetate is preferentially utilized by glias and considered to be a marker of glial metabolism [54], which is associated with event of neuronal survivals [55]. The lower levels of choline, phosphorylcholine and *myo*-inositol in the MCAO models suggest that ischemia has led to disruptions in cell membrane metabolisms since these metabolites are important components of cell membrane phospholipids. This is not surprising since the cerebral ischemia stimulated release of glutamate can activate phospholipases [56]. Such changes of choline agreed well with the observations made in ischemic brain tissues under ischemia for 24 h [16,57]. The reduction of brain osmolytes such as *myo*-inositol is consistent with previous results [34] and may be related to the ischemia-induced changes in local osmolality.

The depletions of hypoxanthine, inosine, xanthine are probably related to ATP catabolism since these are all catabolites of adenosine. Previous results showed that under ischemic conditions, adenosine triphosphate (ATP) was catabolized to adenosine and further to inosine and xanthine [58], which accumulated in the extracellular space in a few minutes post ischemia [59]. However, the elevation of adenosine was only transient and its level began to decrease [32] 3 h after occlusion. Nevertheless, these observations may be also related to the MCAO induced changes in biosynthesis and/or degradations of nucleic acids.

It was interesting to note that three animals in MCAO group failed the relevant neurological evaluations and had more similar

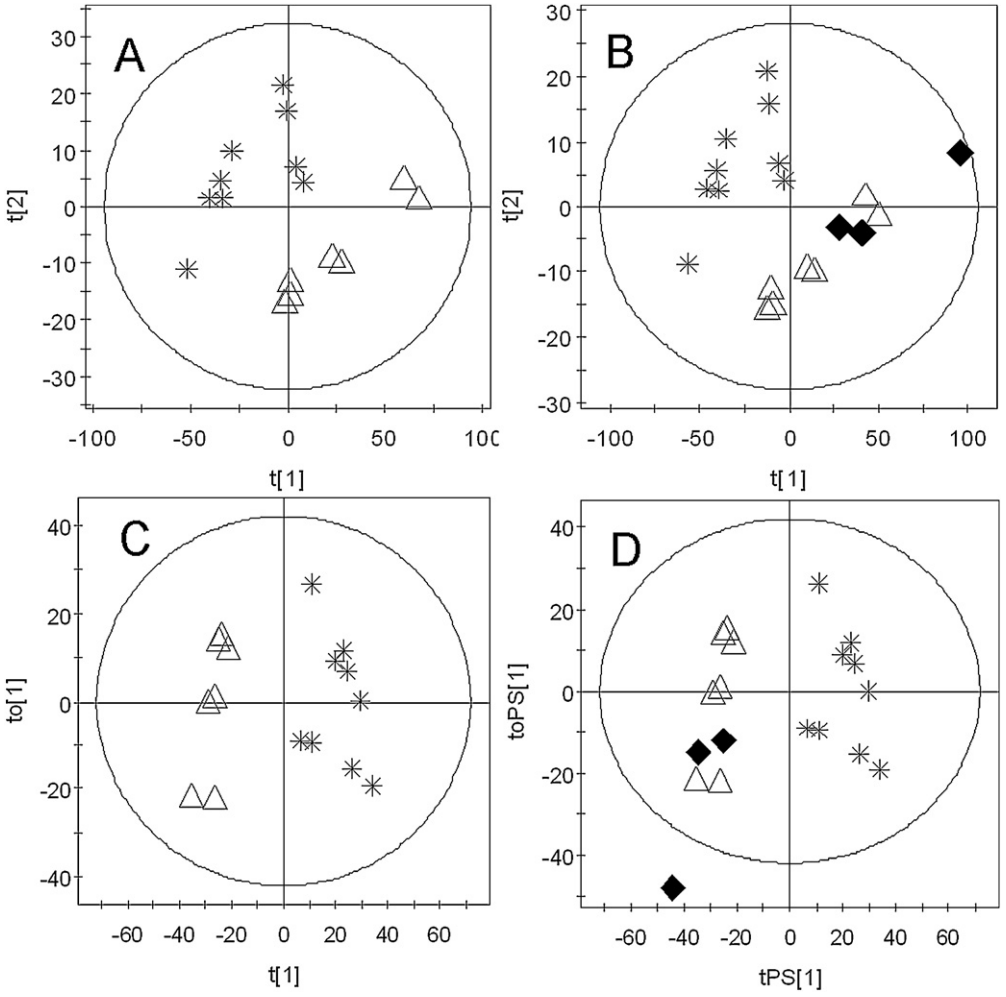

Fig. 2. Scores plots derived from ^{1}H NMR spectra of extracts from right brain tissue of rats in the MCAO (*), sham (△) group and three failed MCAO group members (♦). (A) PCA scores plot for the MCAO and sham group; (B) scores plot from PCA model for MCAO, sham groups and three failed rats; (C) scores plot of OPLS-DA model for MCAO and sham groups; (D) the predictive scores plot from OPLS-DA model in (C) to predict three failed MCAO rats.

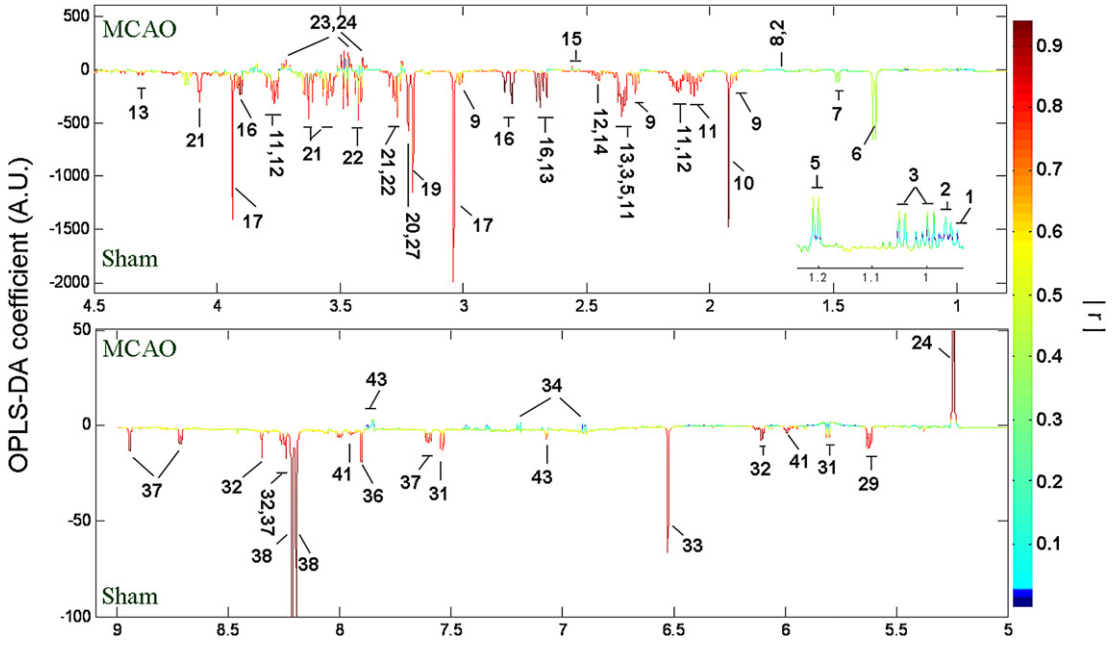

Fig. 3. Coefficient-coded loadings plot for the OPLS-DA model from sham and MCAO groups. Metabolite keys were given in Table 1.

Table 2
Correlation coefficients and relative changes of metabolites responsible for the separation between the sham and MCAO rats.

Metabolites (keys)	^{1}H δ(multiplicity)	MCAO vs sham-operated group OPLS-DA coefficients	p-Value	Relative changes
Acetate(10)	1.92(s)	−0.909	1.4×10^{-6}	−74.1%
Glutamate(11)	2.06(m)	−0.840	1.1×10^{-3}	−48.0%
Glutamine(12)	2.14(m)	−0.844	3.0×10^{-4}	−32.9%
GABA(9)	2.30(t)	−0.737	4.7×10^{-3}	−36.7%
Taurine(22)	3.42(t)	−0.848	1.4×10^{-2}	−34.5%
Aspartate(16)	2.68(dd)	−0.926	1.5×10^{-6}	−75.6%
Malate(13)	2.82(dd)	−0.934	1.2×10^{-6}	−77.9%
Creatine(17)	3.04(s)	−0.875	2.0×10^{-4}	−61.1%
Choline(19)	3.21(s)	−0.824	1.0×10^{-3}	−51.6%
Phosphorylcholine(27)	3.23(s)	−0.864	3.8×10^{-5}	−62.0%
Myo-inositol(21)	3.29(t)	−0.846	2.0×10^{-4}	−53.1%
α-Glucose(24)	5.23(d)	+0.957	8.7×10^{-6}	+566.0%
U2(29)	5.62(dd)	−0.782	3.0×10^{-4}	−74.3%
UDP/UTP*(41)	5.99(d)	−0.903	3.0×10^{-5}	−62.6%
Fumarate(33)	6.53(s)	−0.868	3.4×10^{-5}	−66.7%
Uracil(31)	7.55(d)	−0.826	3.1×10^{-3}	−40.5%
Xanthine(36)	7.90(s)	−0.889	1.0×10^{-3}	−54.1%
Inosine(32)	8.35(s)	−0.839	3.0×10^{-4}	−57.5%
Hypoxanthine(38)	8.20(s)	−0.952	7.8×10^{-7}	−77.4%
Nicotinurate(37)	8.71(dd)	−0.905	3.2×10^{-5}	−63.4%
U3(44)	8.00(d)	−0.749	3.5×10^{-3}	−40.8%

Signs "+" and "−" indicate increase and decrease for the level of metabolites in MCAO related to the sham group. The significance of metabolite changes was determined by a two-side unpaired t-test ($p < 0.05$). Relative changes were calculated as described in Section 2.

* UDP/UTP, uridine diphosphate/uridine triphosphate.

behavior to the sham group. The metabonomic features of these three animals were also more similar to those of the sham-operated rats. This indicates that the metabolic feature analysis is probably a good alternative way for identifying the MCAO conditions and perhaps for assessing the functional outcome in cerebral ischemic studies.

5. Conclusion

Focal cerebral ischemia for 26 h causes systematic rat neurochemistry changes in the metabolic network involving glycolysis, TCA cycles, metabolisms of amino acids, phospholipids and nucleotides. These metabolic changes are associated with the ischemia-caused disruptions to a number of important cerebral functions such as energy productions, glutamate–glutamine cycle and malate–aspartate shuttle. These findings indicate that the NMR-based metabonomic analysis is useful for detecting the occurrence of focal cerebral ischemia which might be useful for disease diagnosis and prognosis for ischemic stroke and probably for other neurodegenerative disorders as well.

Acknowledgements

We acknowledge the financial supports from the Ministry of Science and Technology of China (2010CB912501), National Nature Science Foundation of China (20825520 and 20921004) and Chinese Academy of Sciences (KJCX2-YW-W11, KJCX2-YW-W13).

Appendix A. Supplementary data

Supplementary data associated with this article can be found, in the online version, at doi:10.1016/j.talanta.2011.10.022.

References

[1] K. Strong, C. Mathers, R. Bonita, Lancet Neurol. 6 (2007) 182–187.
[2] http://www.who.int/cardiovascular_diseases.
[3] V.L. Roger, A.S. Go, D.M. Lloyd-Jones, R.J. Adams, J.D. Berry, T.M. Brown, M.R. Camethon, S. Dai, G. de Simone, E.S. Ford, C.S. Fox, H.J. Fullerton, C. Gillespie, K.J. Greenlund, S.M. Hailpem, J.A. Heit, P.M. Ho, V.J. Howard, B.M. Kissela, S.J. Kittner, D.T. Lackland, J.H. Lichtman, L.D. Lisabeth, D.M. Makuc, G.M. Marcus, A. Marelli, D.B. Matchar, M.M. McDermott, J.B. Meigs, C.S. Moy, D. Mozaffarian, M.E. Mussolino, G. Nichol, N.P. Paynter, W.D. Rosamond, P.D. Sorlie, R.S. Stafford, T.N. Turan, M.B. Turner, N.D. Wong, J. Wylie-Rosett, A.H.A.S. Comm, S.S. Subcomm, Circulation 123 (2011) E18–E209.
[4] D.L. Brown, B. Boden-Albala, K.M. Langa, L.D. Lisabeth, M. Fair, M.A. Smith, R.L. Sacco, L.B. Morgenstern, Neurology 67 (2006) 1390–1395.
[5] F. Palm, C. Urbanek, S. Rose, F. Buggle, B. Bode, M.G. Hennerici, K. Schmieder, G. Inselmann, R. Reiter, R. Fleischer, K.O. Piplack, A. Safer, H. Becher, A.J. Grau, Stroke 41 (2010) 1865–1870.
[6] B.K. Siesjo, Neurochem. Pathol. 9 (1988) 31–88.
[7] R. Jin, G.J. Yang, G.H. Li, J. Leukocyte Biol. 87 (2010) 779–789.
[8] J.W. Schmidley, Stroke 21 (1990) 1086–1090.
[9] I. Unal-Cevik, M. Kilinc, A. Can, Y. Gursoy-Ozdemir, T. Dalkara, Stroke 35 (2004) 2189–2194.
[10] P. Lipton, Physiol. Rev. 79 (1999) 1431–1568.
[11] O.P. Ottersen, J.H. Laake, W. Reichelt, F.M. Haug, R. Torp, J. Chem. Neuroanat. 12 (1996) 1–14.
[12] Y. Xie, G. Mies, K.A. Hossmann, Stroke 20 (1989) 620–626.
[13] S.R. Felber, F.T. Aichner, R. Sauter, F. Gerstenbrand, Stroke 23 (1992) 1106–1110.
[14] D.E. Saunders, Brit. Med. Bull. 56 (2000) 334–345.
[15] G.D. Graham, A.M. Blamire, A.M. Howseman, D.L. Rothman, P.B. Fayad, L.M. Brass, O.A.C. Petroff, R.G. Shulman, J.W. Prichard, Stroke 23 (1992) 333–340.
[16] A. vanderToorn, R.M. Dijkhuizen, C.A.F. Tulleken, K. Nicolay, Magn. Reson. Med. 36 (1996) 914–922.
[17] Z. Ramadan, D. Jacobs, M. Grigorov, S. Kochhar, Talanta 68 (2006) 1683–1691.
[18] S. Wold, K. Esbensen, P. Geladi, Chemometr. Intell. Lab. Syst. 2 (1987) 37–52.
[19] M. Bylesjo, M. Rantalainen, O. Cloarec, J.K. Nicholson, E. Holmes, J. Trygg, J. Chemometr. 20 (2006) 341–351.
[20] H.R. Tang, Y.L. Wang, Prog. Biochem. Biophys. 33 (2006) 401–417.
[21] J.K. Nicholson, J.C. Lindon, E. Holmes, Xenobiotica 29 (1999) 1181–1189.
[22] M. Arjmand, M. Kompany-Zareh, M. Vasighi, N. Parvizzadeh, Z. Zamani, F. Nazgooei, Talanta 81 (2010) 1229–1236.
[23] Y.L. Wang, J. Utzinger, J. Saric, J.V. Li, J. Burckhardt, S. Dirnhofer, J.K. Nicholson, B.H. Singer, R. Brun, E. Holmes, Proc. Natl. Acad. Sci. U.S.A. 105 (2008) 6127–6132.
[24] X.Y. Zhang, Y.L. Wang, F.H. Hao, X.H. Zhou, X.Y. Han, L.N. Ji, H.R. Tang, J. Proteome Res. 8 (2009) 5188–5195.
[25] Y.X. Yang, C.L. Li, X. Nie, X.S. Feng, W.X. Chen, Y. Yue, F. Deng, H.R. Tang, J. Proteome Res. 6 (2007) 2605–2614.
[26] M.S. Sabatine, E. Liu, D.A. Morrow, E. Heller, R. McCarroll, R. Wiegand, G.F. Berriz, F.P. Roth, R.E. Gerszten, Circulation 112 (2005) 3868–3875.
[27] J.F. Wu, E. Holmes, J. Xue, S.H. Xiao, B.H. Singer, H.R. Tang, J. Utzinger, Y.L. Wang, Int. J. Parasitol. 40 (2010) 695–703.
[28] R. Madsen, T. Lundstedt, J. Trygg, Anal. Chim. Acta 659 (2010) 23–33.
[29] J.K. Nicholson, J. Connelly, J.C. Lindon, E. Holmes, Nat. Rev. Drug Discov. 1 (2002) 153–161.
[30] D.G. Robertson, Toxicol. Sci. 85 (2005) 809–822.
[31] L.M. Zhang, Y.F. Ye, Y.P. An, Y.A. Tian, Y.L. Wang, H.R. Tang, J. Proteome Res. 10 (2011) 614–623.
[32] A. Melani, L. Pantoni, C. Corsi, L. Bianchi, A. Monopoli, R. Bertorelli, G. Pepeu, F. Pedata, Stroke 30 (1999) 2448–2454.
[33] L. Hillered, Z. Kotwica, U. Ungerstedt, Res. Exp. Med. (Berl.) 191 (1991) 219–225.
[34] M. Nonaka, T. Yoshimine, E. Kohmura, A. Wakayama, T. Yamashita, T. Hayakawa, J. Neurol. Sci. 157 (1998) 25–30.

[35] M. Nonaka, T. Yoshimine, E. Kumura, E. Kohmura, A. Wakayama, T. Hayakawa, Neurol. Res. 21 (1999) 771–774.
[36] A.K. Haberg, H. Qu, U. Sonnewald, J. Neurochem. 109 (2009) 174–181.
[37] C.N. Xiao, F.H. Hao, X.R. Qin, Y.L. Wang, H.R. Tang, Analyst 134 (2009) 916–925.
[38] T. Shimazu, I. Inoue, N. Araki, Y. Asano, M. Sawada, D. Furuya, H. Nagoya, J.H. Greenberg, Stroke 36 (2005) 353–359.
[39] E.Z. Longa, P.R. Weinstein, S. Carlson, R. Cummins, Stroke 20 (1989) 84–91.
[40] J. Trygg, S. Wold, J. Chemometr. 16 (2002) 119–128.
[41] E.J.L. Eriksson, N. Kettaneh-Wold, J. Trygg, C. Wikström, S. Wold, Multi- and Megavariate Data Analysis. Part I. Basic Principles and Applications, 2nd ed., Umetrics Academy, Umea, Sweden, 2006.
[42] L. Eriksson, J. Trygg, S. Wold, J. Chemometr. 22 (2008) 594–600.
[43] O. Cloarec, M.E. Dumas, J. Trygg, A. Craig, R.H. Barton, J.C. Lindon, J.K. Nicholson, E. Holmes, Anal. Chem. 77 (2005) 517–526.
[44] J.K. Nicholson, P.J.D. Foxall, M. Spraul, R.D. Farrant, J.C. Lindon, Anal. Chem. 67 (1995) 793–811.
[45] W.M.T. Fan, Prog. Nucl. Magn. Reson. Spectrosc. 28 (1996) 161–219.
[46] D.S. Wishart, C. Knox, A.C. Guo, R. Eisner, N. Young, B. Gautam, D.D. Hau, N. Psychogios, E. Dong, S. Bouatra, R. Mandal, I. Sinelnikov, J.G. Xia, L. Jia, J.A. Cruz, E. Lim, C.A. Sobsey, S. Shrivastava, P. Huang, P. Liu, L. Fang, J. Peng, R. Fradette, D. Cheng, D. Tzur, M. Clements, A. Lewis, A. De Souza, A. Zuniga, M. Dawe, Y.P. Xiong, D. Clive, R. Greiner, A. Nazyrova, R. Shaykhutdinov, L. Li, H.J. Vogel, I. Forsythe, Nucleic Acids Res. 37 (2009) D603–D610.
[47] K. Katsura, E.B.R. Deturco, J. Folbergrova, N.G. Bazan, B.K. Siesjo, J. Neurochem. 61 (1993) 1677–1684.
[48] H. Igarashi, I.L. Kwee, T. Nakada, Y. Katayama, A. Terashi, Brain Res. 907 (2001) 208–221.
[49] M. Baumann, E. Bender, G. Stommer, G. Gross, K. Brand, Mol. Cell. Biochem. 87 (1989) 137–145.
[50] H. Kita, K. Shima, M. Tatsumi, H. Chigasaki, J. Cereb, Blood Flow Metab. 15 (1995) 235–241.
[51] S.H. Graham, J. Chen, F.R. Sharp, R.P. Simon, J. Cereb, Blood Flow Metab. 13 (1993) 88–97.
[52] J.M. Pascual, F. Carceller, J.M. Roda, S. Cerdan, Stroke 29 (1998) 1048–1056.
[53] M. Sun, C. Xu, Cell. Mol. Neurobiol. 28 (2008) 593–611.
[54] R.A. Waniewski, D.L. Martin, J. Neurosci. 18 (1998) 5225–5233.
[55] A. Håberga, U. Sonnewald, H. Leif, Advances in Molecular and Cell Biology, Elsevier, 2003, pp. 837–855.
[56] R.M. Adibhatla, J.F. Hatcher, R.J. Dempsey, AAPS J. 8 (2006) E314–E321.
[57] A. vanderToorn, R.M. Dijkhuizen, C.A.F. Tulleken, K. Nicolay, NMR Biomed. 8 (1995) 245–252.
[58] C. Barsotti, P.L. Ipata, Int. J. Biochem. Cell Biol. 36 (2004) 2214–2225.
[59] H. Hagberg, P. Andersson, J. Lacarewicz, I. Jacobson, S. Butcher, M. Sandberg, J. Neurochem. 49 (1987) 227–231.
[60] H. Dai, C.N. Xiao, H.B. Liu, H.R. Tang, J. Proteome Res. 9 (2010) 1460–1475.
[61] H. Dai, C.N. Xiao, H.B. Liu, F.H. Hao, H.R. Tang, J. Proteome Res. 9 (2010) 1565–1578.